International Journal of Thermal Sciences 48 (2009) 2148–2158

Contents lists available at ScienceDirect

International Journal of Thermal Sciences

journal homepage: www.elsevier.com/locate/ijts

Thermal performance criteria of elliptic tube bundle in crossflow

Talaat A. Ibrahim [a], Abdalla Gomaa [b,*]

[a] King Saud University, P.O. 70908, Riyadh 11577, Saudi Arabia
[b] Abdalla Gomaa Refrigeration and Air-conditioning Dept., Faculty of Industrial Education, Helwan University, El-Sawah Street, Cairo 11887, Egypt

ARTICLE INFO

Article history:
Received 3 July 2008
Received in revised form
15 March 2009
Accepted 16 March 2009
Available online 24 April 2009

Keywords:
Thermal performance criteria
Turbulent flow
Elliptic tube bundle

ABSTRACT

In this work, the thermofluid characteristics of the elliptic tube bundle in crossflow have been investigated. Experimental and numerical investigations of the turbulent flow through bundle of elliptic tubes heat exchanger are carried out with a particular reference to the circular tube bundle. The investigation covers the effects of key design parameters of Reynolds numbers (5600–40,000), minor-to-major axis ratios (0.25, 0.33. 0.5 and 1) and flow angles of attack (0–150°). Five bundles of elliptic tube heat exchangers with different axis ratios were designed and manufactured in staggered manner. Numerical CFD modeling using finite volume discretization method was conducted to predict the system performance extensively. Four methods were presented to resort a metric that expresses the thermal performance criteria of the elliptic tube bundle. The results indicated that, increasing the angle of attack clockwise until 90° enhances the convective heat transfer coefficient considerably. The maximum thermal performance under constraint of a fixed pumping power or a mass flow rate was obtained at a zero angle of attack and the minimum thermal performance occurred at an angle of attack equals 90°. The best thermal performance of the elliptic tube heat exchanger was qualified with the lower values of Reynolds number, axis ratio and angle of attack.

1. Introduction

The increase in energy demand in all sectors of the human society requires an increasingly more intelligent use of available energy. Many industrial applications require the use of heat exchangers with different tubes' arrangements, either finned or non-finned, as in air conditioning systems, refrigeration, heaters, radiators, etc. Such devices have to be compact, lightweight and high performance. Crossflow heat exchanger with elliptic tube arrangement is receiving increase attentions that produce enhanced heat transfer surface compared with circular tube arrangement. It is important at the outset to recognize that the enhancement of heat transfer can lead to an increase in pumping power. As a result, it is very important to determine the evaluation criteria that can be developed to obtain the performance of the heat exchange devices based on the trade between the enhancement of the heat transfer and the cost of pumping power.

There are a number of studies dealing with the performance of the elliptic tubes heat exchanger in crossflow. Terukazu et al. [1] encompassed the flow in the neighborhood of an elliptic cylinder with an axis ratio of 0.33. They concluded that the elliptical tube performs better than the circular configuration in terms of reduced drag coefficient and pressure drop. Jang and Li [2] performed a numerical analysis of two-dimensional laminar flow over an elliptic tube bank. They concluded that a higher thermal performance achieved by elliptic tube bank and an appropriate arrangement of the elliptic tube enhances the heat transfer performance of the tube bank. Rocha et al. [3] found the elliptical configuration with axis ratio of 0.86 and a ratio of semi-minor axis to the length of tube row of 0.23 is the most efficient one. This is for a constant Prandtl number of 0.70 and Reynolds number ranged from zero to 1600. Badr [4] investigated a numerical study on the effects of axis ratio and angle of attack on the heat transfer at constant surface temperature of a single elliptical cylinder. Reynolds number was varied from 20 to 500. The maximum Nusselt number was found to be occurred at zero angle of attack and at small axis ratio. Matos et al. [5] reported a 13% relative heat transfer gain due to elliptic configuration for the same flow obstruction cross-sectional area with an axis ratio of 0.75 and Reynolds number ranges from 300 to 800.

Bouris et al. [6] studied a numerical evaluation of alternate tube configurations for particles deposition rate reduction for inline tube bundles. They found that the elliptic tube has a promising indication to allow an increase in the transfer surface area and a reduction in the pressure drop. Harris and Goldschmidt [7] investigated the effects of axis ratio and angle of attack on the overall heat transfer from combustion gases confined within an elliptical tube heat

* Corresponding author. Tel.: +20 0106826231.
E-mail address: abdallagomaa@hotmail.com (A. Gomaa).

1290-0729/$ – see front matter © 2009 Elsevier Masson SAS. All rights reserved.
doi:10.1016/j.ijthermalsci.2009.03.011

Nomenclature

a	ellipse minor axis, m
A_f	face area of the cell, m^2
A_{ff}	free flow area, m^2
A_{fr}	frontal area, m^2
A_{GF}	area goodness factor, dimensionless
A_r	axis ratio (a/b), dimensionless
A_s	transfer surface area, m^2
b	ellipse major axis, m
C_p	specific heat, $J\,kg^{-1}\,K^{-1}$
D	circular tube diameter, m
D_h	hydraulic diameter, m
f	friction factor, dimensionless
h	heat transfer coefficient, $W\,m^{-2}\,K^{-1}$
j	heat transfer Colburn factor, dimensionless
k	thermal conductivity, $W\,m^{-1}\,K^{-1}$
$\dot{m}$	mass flow rate, $kg\,s^{-1}$
N_R	number of tube rows, dimensionless
Nu	Nusselt number (hD_h/k), dimensionless
Pr	Prandtl number ($C_p\mu/k$), dimensionless
R	measured parameter
Re	Reynolds number ($\rho u D_h/\mu$), dimensionless
S_L	longitudinal tube-pitch, m
S_t	transverse tube-pitch, m
St	Stanton number ($Nu/RePr$), dimensionless
T	temperature, °C
$\boldsymbol{u}$	velocity vector ($u_i + v_j + w_k$), $m\,s^{-1}$
u_{max}	air velocity at minimum free flow area, $m\,s^{-1}$
V	volume, m^3

Greek symbols

α	angle of attack, degree
Δp	pressure drop, $N\,m^{-2}$
ε	heat transfer per unit pumping power, dimensionless
η	efficiency index, dimensionless
μ	dynamic viscosity, $N\,s\,m^{-2}$
q	logarithmic mean temperature difference, K
ρ	density, $kg\,m^{-3}$
σ	contraction ratio, A_{ff}/A_f

Subscripts

a	air
av	average
CV	control-volume
eff	effective
i	inlet
max	maximum
o	outlet
w	water

exchanger. They concluded that, an axis ratio of 0.30 or less should be achieved to realize any appreciable change in the overall heat transfer coefficient (10%) over the circular tube. Khan et al. [8] studied the forced convection heat transfer on one inline of elliptic tubes row with an axis ratio of 0.33 and at zero angle of attack. The results revealed that the heat transfer rate increased with the increase of both water and air flows. A three-dimensional numerical and experimental geometric optimization investigation to maximize the forced convection heat transfer rate between a bundle of finned tubes was carried out by Matos et al. [9,10]. The studies were conducted for circular and elliptic configurations with 12 tubes. Air was used as external fluid in the laminar flow regime for $Re = 852$ and 1065. In addition, the tube-to tube spacing, eccentricity and fin-to-fin spacing were investigated in the heat exchanger geometry. A heat transfer gain up to 20% was reported for the optimal elliptic arrangement in compared to the optimal circular one.

Li et al. [11] studied the two-dimensional computational modeling of the elliptical tubes with axis ratios of 0.3, 0.5, and 0.8. Laminar flow was assumed with Reynolds number ranged from 500 to 10,000 and a constant surface temperature. They concluded that the elliptical cylinder with an axis ratio of 0.5 and zero angle of attack reduces the pressure drop by 30–40% compared with a circular cylinder while Nusselt number was found to be 15% lower than the circular tube.

Li et al. [12] treated the fluid flow inside the elliptic tube. They studied the friction factor and the heat transfer of the fully developed flow inside an elliptic tube configuration. Results indicated that the heat transfer performance of the elliptic tube is much better than for round tube under a constant pumping power. Recently, Tao et al. [13] investigated numerically the laminar heat transfer and fluid flow characteristics for circular and elliptic tube arrangements. They concluded that a 30% gain of the heat transfer and consequently 10% increasing in the friction factor have been obtained.

From the preceding review, the performance evaluation criteria of the elliptic tube heat exchanger with the key design parameters are not presented. However, numerous factors that affect the performance of heat exchangers may be designed to provide different performance criteria; this has motivated the present investigation. A local point of this work is the thermal performance criteria under the constraint of a constant pumping power or mass flow rate, which includes possible enhancement of the heat transfer or a possible reduction of the heat exchanger size for a given duty or a possible reduction of the temperature difference approach. To achieve these goals, experimental and numerical studies of heat transfer characteristics over an elliptic tube bundle in crossflow are investigated in turbulent flow regime. The investigation covers the effects of wide ranges of key design parameters involving Reynolds number ($Re = 5300$–$40{,}000$), minor-to-major axis ratio ($A_r = 0.25$, 0.33. 0.5 and 1) and flow angle of attack ($\alpha = 0°$, 30°, 60°, 90°, 120° and 150°). Four methods are presented to resort a metric that expresses the thermal performance criteria of the elliptic tube bundle with the particular reference of the traditional circular tube bundle. These methods are depending on what is held fixed (heat duty, mass flow rate and pressure drop) and what is the desired objective (heat transfer enhancement, frontal area and pumping power reduction).

2. Experimental apparatus and procedures

The experiments were conducted in a Plexiglas wind tunnel. The experimental test rig consists of a square duct of 0.3 m × 0.3 m and 5 m length equipped with a suction centrifugal fan as shown in Fig. 1. The fan has a power of 3.67 kW and it was linked with a variable speed inverter having a capability to fine tuning the air velocity. The average air velocity in the test section is varied from 3.8 m/s to 20 m/s corresponding to Reynolds number of 5300–28,000, respectively.

Four elliptic tubes' bundles with different axis ratios ($A_r = 0.25$, 0.333, 0.5 and 0.666) in addition to a circular tube bundle ($A_r = 1$) were designed and manufactured in staggered manner. The tubes were connected with two copper headers located at the top and the bottom of the bundle to form one unit of a heat exchanger. The tube arrays (Fig. 2a) were constructed to be 5 × 5 rows with transverse

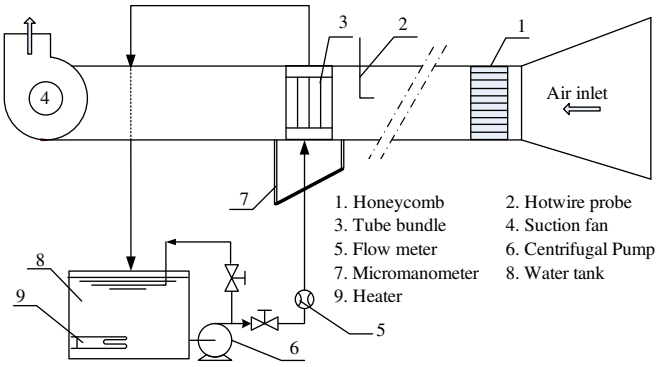

Fig. 1. Schematic diagram of the experimental test rig.

tube-pitch ($S_t = 0.03$ m), longitudinal tube-pitch ($S_L = 0.026$ m), equivalent to a circular tube diameter ($D = 0.0127$ m) and tube length = 0.2 m, as a typical design of Thermal Transfer Technology LTD.

The tube arrays were fixed in the test section with a special mechanism having the capability of changing the angle of attack. The angle of attack, as illustrated in Fig. 2b, was adjusted by turning the tube arrays around a vertical axis at the center of a flat surface from 0° to 150° (0°, 30°, 60°, 90°, 120° and 150°) using a protractor mechanism. Details of the elliptic tube configurations are presented in Table 1. The tube bundle was heated by hot water that was supplied from an electric boiler using a centrifugal pump of 0.55 kW.

2.1. Measuring techniques

The hot water was controlled and supplied to the heat exchanger with a temperature of 80 ± 2 °C. The inlet and the outlet temperatures of the waterside were measured using four shelled pre-calibrated k-type thermocouples. A three and nine grid points of the k-type thermocouple probes were fixed on the upstream and downstream of the test section, respectively to measure the air temperature. All thermocouples were connected via switching box to a digital thermometer. The water flow rate was measured using a flowmeter. The velocity profile of the air through the duct section was identified by hotwire anemometer. The pressure drop across the heat exchanger was measured using digital micromanometer. Sufficient time was allowed to get the experimental measuring parameters stabilization, which was observed to be about 40–50 min.

2.2. Measurements' uncertainties

The experimental error analysis indicates the implication of error of the measured parameters on the uncertainty of the results. A detailed analysis of the various experimental uncertainties is carried out using the differential approximation method for error analysis [14]. The maximum uncertainties in measuring parameters under investigation are: temperature ±1.23%, air velocity through the duct section, pressure drop across the heat exchanger and water volume flow rate ±4.84%, ±1.21% and 1.43%, respectively. However, the maximum uncertainties of the results that have been obtained from the measured parameters for heat transfer coefficient, Nusselt number, friction factor and heat transfer per unit pumping power are ±12.5%, ±12.5%, ±11.2% and ±10.3%, respectively.

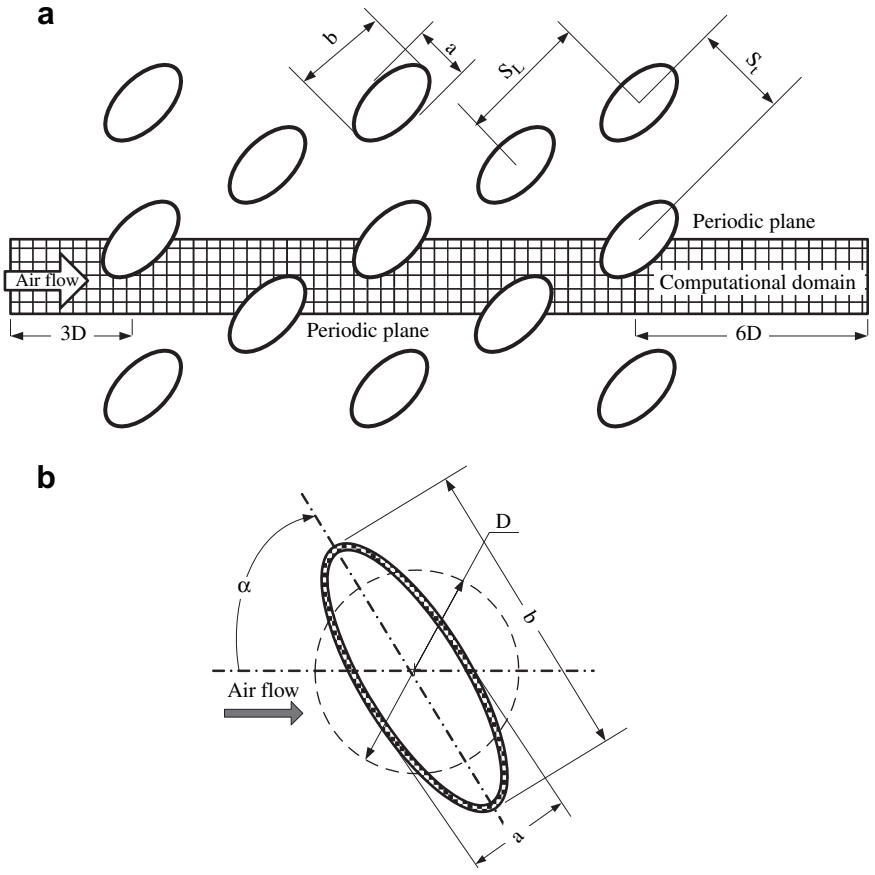

Fig. 2. (a) Schematic diagram of the elliptic tube bundle heat exchanger. (b) Elliptic tube details.

Table 1
Details of the elliptic tube configurations.

Specimen no.	a (mm)	b (mm)	A_r	α (degree)	Re, experimental	Re, numerical
Circular	6.4	6.4	1	0°	5300–28,000	5600–40,000
Elliptic I	5.2	7.8	0.66	0°, 30°, 60°, 90°, 120° and 150°	5300–28,000	5600–40,000
Elliptic II	4.5	9	0.5	0°, 30°, 60°, 90°, 120° and 150°	5300–28,000	5600–40,000
Elliptic III	3.7	11	0.33	0°, 30°, 60°, 90°, 120° and 150°	5300–28,000	5600–40,000
Elliptic IV	3.2	12.7	0.25	0°, 30°, 60°, 90°, 120° and 150°	5300–28,000	5600–40,000

3. Mathematical model

The governing equations that describe the airflow through the tube arrays are a set of non-linear partial differential equations (PDEs). The airflow is governed by the mass, the momentum and the energy equations. A finite volume discretization method using a SIMPLEC-based solution algorithm of the velocity–pressure coupling was applied with a segregated solver. The numerical modeling of the turbulent flow through the tube bundle heat exchanger was solved using FLUENT-6.2 CFD program. The momentum and energy equations were solved by the second order upwind scheme. The airflow and the heat transfer through the tube arrays were treated using k–ε RNG "renormalization group" turbulence model. The RNG model is accurate and reliable for a wider class of flow than the standard k–ε model [15]. The transport equations of the RNG k–ε model are given by the following equations:

$$\frac{\partial}{\partial t}(\rho k)+\frac{\partial}{\partial x_i}(\rho k u_i)=\frac{\partial}{\partial x_j}\left(\alpha_k \mu_{\text{eff}}\frac{\partial k}{\partial x_j}\right)+G_k+G_b-\rho\varepsilon+S_k \tag{1}$$

$$\frac{\partial}{\partial t}(\rho\varepsilon)+\frac{\partial}{\partial x_i}(\rho\varepsilon u_i)=\frac{\partial}{\partial x_j}\left(\alpha_\varepsilon \mu_{\text{eff}}\frac{\partial \varepsilon}{\partial x_j}\right)+C_{1\varepsilon}\frac{\varepsilon}{k}(G_k+C_{3\varepsilon}G_b)-C_{2\varepsilon}\rho\frac{\varepsilon^2}{k}-R_\varepsilon+S_k \tag{2}$$

where

$$G_k=-\rho\overline{u_i'u_j'}\frac{\partial u_j}{\partial x_i},\quad R_\varepsilon=\frac{C_\mu\rho\xi^3(1-\xi/\xi_o)}{1+\theta\xi^3}\frac{\varepsilon^2}{k}$$

$$G_b=g_i\frac{\mu_t}{\rho Pr_t}\frac{\partial\rho}{\partial x_i},\quad C_{3\varepsilon}=\tanh\left|\frac{v}{u}\right|,\quad S_k=\xi\varepsilon$$

The model constants $C_{1\varepsilon}$, $C_{2\varepsilon}$, α_k, α_ε, ξ_o and θ in Eqs. (2) and (3) are

$$C_{1\varepsilon}=1.42,\ C_{2\varepsilon}=1.68,\ \alpha_k=\alpha_\varepsilon\approx 1.393,\ \xi_o=4.34,\ \text{and}\ \theta=0.012$$

The term G_k represents the generation of turbulence kinetic energy due to the mean velocity gradients and G_b describes the generation of turbulence kinetic energy due to buoyancy. The quantities of α_k and α_ε are the inverse of Prandtl numbers for both k and ε, respectively.

The numerical solution transforms the set of partial differential equations into a discretised algebraic form and solves them to obtain a set of flow-field values at discretised points in time and space. The discretised form of a non-linear governing equation is linearised to produce a system of equation for the dependent variables in every computational cell. The resultant linear system is then solved to yield an updated flow-field solution. For a given variable, the unknown value in each cell is computed using a relation that includes both the existing and the unknown values from neighboring cells. Therefore, each unknown will appear in more than one equation in the system, and these equations must be solved simultaneously to give the unknown quantities. The computational domain is discretised into a set of control volumes, which are arranged into a grid as illustrated in Fig. 3.

The governing equations can be expressed in a general form of a general variable φ as presented in the following equation:

$$\frac{\partial(\rho\varphi)}{\partial t}+\text{div}(\rho\varphi u)=\text{div}(\Gamma\ \text{grad}\ \varphi)+S_\varphi \tag{3}$$

where $\partial(\rho\varphi)/\partial t$ is the rate of the change of variable φ, $\text{div}(\rho\varphi u)$ is the convective term, $\text{div}(\Gamma\ \text{grad}\ \varphi)$ is the diffusive term and S_φ is the source term.

This general equation can describe the mass, momentum and energy equations of the airflow by setting the general variable φ equal to 1, (u,v,w) and T, respectively. This equation is used as a starting point for the computational procedures. Discretization of the governing equations can be illustrated by considering the integration of Eq. (3) on a control-volume representing Eq. (4).

$$\int_{CV}\frac{\partial(\rho\varphi)}{\partial t}+\int_{CV}\text{div}(\rho\varphi u)=\int_{CV}\text{div}(\Gamma\ \text{grad}\ \varphi)+\int_{CV}S_\varphi \tag{4}$$

Eq. (5) is applied to each cell in the domain, which yields algebraic equation on a given cell.

$$\sum_{f}^{N_{\text{faces}}}u_f\varphi_f A_f=\sum_{f}^{N_{\text{faces}}}\Gamma_\varphi(\text{div}\ \varphi)_n A_f+S_\varphi V \tag{5}$$

Preliminary simulation was carried out with different grid densities in order to get a grid-independent solution. Considering both accuracy and economics of the solution, computations were performed with a grid-cell size of 0.1 mm (30,000 nodes). Solution with adaptive-grid refinement of hanging nodes technique was adopted to increase grid density based on the evolving flow field,

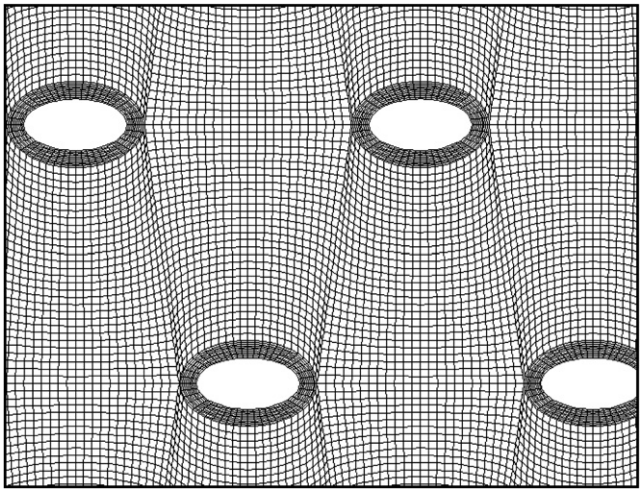

Fig. 3. Adaptive meshing of the numerical model.

and thus provides the potential for more economical use of grid points as shown in Fig. 3. The convergence criterion for all runs was specified to be less than 10^{-4}.

3.1. Boundary conditions

The numerical solution of the turbulent flow through the tube bundle array was treated as steady, incompressible and two-dimensional with neglecting the buoyancy force. The hatched area in Fig. 2a designates the computational domain, where periodic conditions were specified on the midplane of two successive rows of the domain. The periodic condition presented in the problem allows the computational time to be reduced. In order to apply periodic boundaries, a mesh hard link between the identical pair of faces to which the boundary condition was created as indicated in Fig. 2a. At the upstream boundary that located three times of the circular tube diameter ($3D$), a uniform flow velocity was specified. At the downstream boundary that located six times of the circular tube diameter ($6D$), the pressure was set to be zero. However, at the solid surfaces, no-slip conditions as well as constant wall heat flux were specified [5].

3.2. Data reduction

In the experiment, the steady state flow condition was assumed. The fluid properties for both air and water were determined at a mean film temperature. A heat balance on the test section control-volume was performed. The waterside heat transfer coefficient as well as the friction factor is calculated from the correlations mentioned in Eq. (6) [16].

$$h_w = \left(\frac{k_w}{D_w}\right)\frac{(Re_{D_w}-1000)Pr_w(f_w/8)}{1+12.7\sqrt{f_w/8}(Pr_w^{2/3}-1)},$$
$$f_w = (0.79\ln(Re_{D_w})-1.64)^{-2} \quad (6)$$

The airside heat transfer coefficient and the average Nusselt number in the airside can be obtained from Eq. (7) and Eq. (8), respectively.

$$h_a = \frac{\dot{m}_a C_{p_a}(T_{ao}-T_{ai})}{A_s\theta}, \quad \theta = \frac{(T_{wi}-T_{ai})-(T_{wo}-T_{ao})}{\ln((T_{wi}-T_{ai})/(T_{wo}-T_{ao}))} \quad (7)$$

$$Nu = \frac{h_a D_h}{k_a} \quad (8)$$

The hydraulic diameter is justified as an equivalent circular diameter of the elliptic tube [6] and consequently the Reynolds number (Re) and the heat transfer Stanton number (St) are acquired. Another quantity characterizing the flow across the tube arrays is the friction factor, Eq. (9) [17].

$$f = \frac{2\Delta P}{\rho u_{max}^2 N_R} \quad (9)$$

The temperature and the pressure at any section of the numerical model can be computed numerically from the following equation:

$$T = \frac{\int T\rho\vec{u}\cdot d\vec{A}}{\int \rho\vec{u}\cdot d\vec{A}}, \quad p = \frac{\int p\rho\vec{u}\cdot d\vec{A}}{\int \rho\vec{u}\cdot d\vec{A}} \quad (10)$$

4. Results and discussion

The velocity vector plots across both the circular and the elliptic tube bundle with the angle of attack $\alpha = 0^\circ$, 60° and 90° are illustrated in Fig. 4. The airflow is strongly accelerated in the passages between two tubes with maximum velocities lateral to the deeper rows of the elliptic tube bundle. Comparing with the circular tube, the elliptic tube with $\alpha = 0^\circ$ is characterized by less drag due to its better aerodynamic shape which offers lower hydraulic resistance. The airflow separation at the circular tube surface is started at early stage than that of the elliptic tube with $\alpha = 0^\circ$.

As the angle of attack increases from 0° to 60° and to 90°, the air leaves the first row as jets, which possessing a great amount of momentum at a fixed axis ratio. The tubes of the second row lie in the axis of these jets, which accelerated and redirected the jet streams to the inter-passage of the next rows. This condition increases the level of turbulence through the tube array passage and forming vortex shedding which enhances the heat transfer coefficient, however higher pressure drop is expected. The effects of the vortex formation and shedding on the velocity and thermal fields are more pronounced in the case when the angle of attack tends to be a right angle with a lower value of the axis ratio.

The turbulent kinetic energy increases as the angle of attack increases clockwise direction until $\alpha = 90^\circ$. Fig. 5 represents the turbulent kinetic energy per unit mass of the elliptic tube array with $\alpha = 0^\circ$ and 90°, respectively. It was found that the maximum values of the turbulent kinetic energy are taken place at the angle of attack $\alpha = 90^\circ$, while the minimum values occurred at $\alpha = 0^\circ$. At the angle $\alpha > 0^\circ$, the turbulence kinetic energy was larger in magnitude in the case of the lower axis ratio and higher Reynolds number. This, in turn, enhances the convective heat transfer coefficient and consequently increases Nusselt number.

4.1. Thermal performance

The numerical results of Nusselt number and the friction factor were validated against the corresponding experimental results. For clarity, samples of these validations are presented in Fig. 6b and Fig. 8a. There is a good agreement between the experimental and the numerical results and the differences may be attributed to the uncertainties of the measuring instruments.

The Nusselt number versus Reynolds number for the angle of attack ($\alpha = 0^\circ$, 30°, 60°, 90°, 120° and 150°) and for axis ratio ($A_r = 0.5$ and 0.25) involving experimental and numerical results is illustrated in Fig. 6a and b, respectively. At the axis ratio $= 0.5$, the average Nusselt number for the angle of attack $\alpha = 90^\circ$ is greater than that of $\alpha = 0^\circ$ and 30° by 30.5% and 18%, respectively. Comparing with the circular tube array, Nusselt number of the elliptic tubes is higher than that of circular tubes by 17% and 19% for angle of attack $\alpha = 60^\circ$ and 90°, respectively. At a zero angle of attack, Nusselt number is 14% lower than that of the circular tube array. At a certain axis ratio, Nusselt number increases as the angle of attack increases from 0° to 90°, then Nusselt number decreases as the angle of attack ranges $90^\circ < \alpha < 180^\circ$ as shown in Fig. 7.

At a certain Reynolds number, the highest value of Nusselt number occurred at $\alpha = 90^\circ$ while the lowest value is obtained at $\alpha = 0^\circ$. It can be seen that, the Nusselt number decreases when the angle of attack deviates from 90°. For all values of Reynolds numbers with the axis ratio $A_r = 0.5$, the variations of Nusselt numbers are gradually smooth. However, at $A_r = 0.25$, a bell shape can be observed. This can be attributed to the level of turbulence intensity and the induced secondary flow which is more pronounced when the tube tends to be more flat ($A_r < 0.5$) with the angle of attack $\alpha > 0^\circ$. The angle of attack affects the flow mixing positively due to the change of the free flow area and a good flow

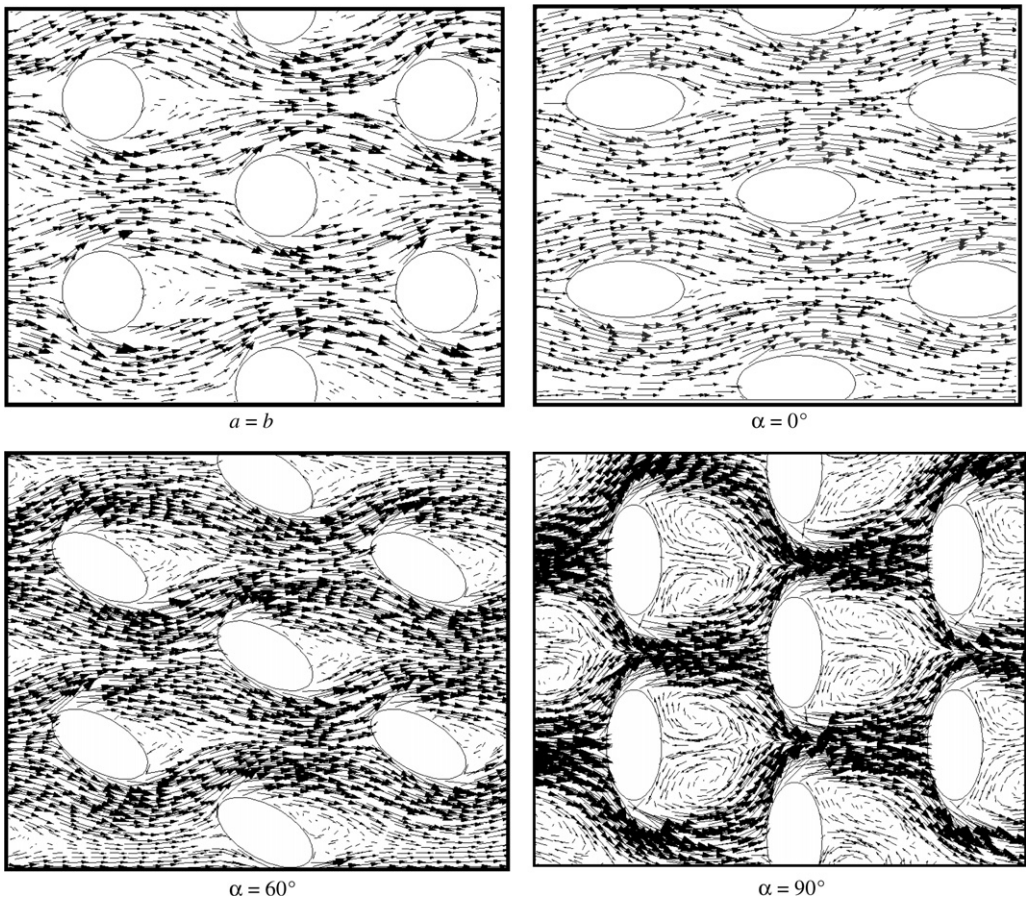

Fig. 4. Velocity field at different angles of attack and $Re = 17{,}000$.

mixing that occurred at the angle of attack tends to be right angle. This can interpret the increase of Nusselt number with the angle of attack however; a higher flow resistance is expected.

The effects of the flow angle of attack on the friction factor at a certain values of the axis ratio ($A_r = 0.25$ and 0.5) are depicted in Fig. 8. At a certain axis ratio, the friction factor increases with the angle of attack when it ranges $0° \le \alpha \le 90°$, then it decreases as angle of attack ranges $90° < \alpha < 180°$. The increase in the friction factor with higher values of the angles of attack is due to the increase of the airflow resistance that occurred when the angle of attack tends to be right angle.

At an axis ratio of 0.5, the friction factor for angle of attack $\alpha = 90°$ is greater than that of $\alpha = 0°$ and 30° by 92% and 80%, respectively. Comparing with the circular tube array ($A_r = 1$), the friction factor of elliptic tubes with the angle of attack $\alpha = 60°$ and 90° is higher than that of circular tubes by 55% and 65%, respectively. At the angle of attack, $\alpha = 0°$, the friction factor is 79% lower than the circular tube array. This can be attributed to the better

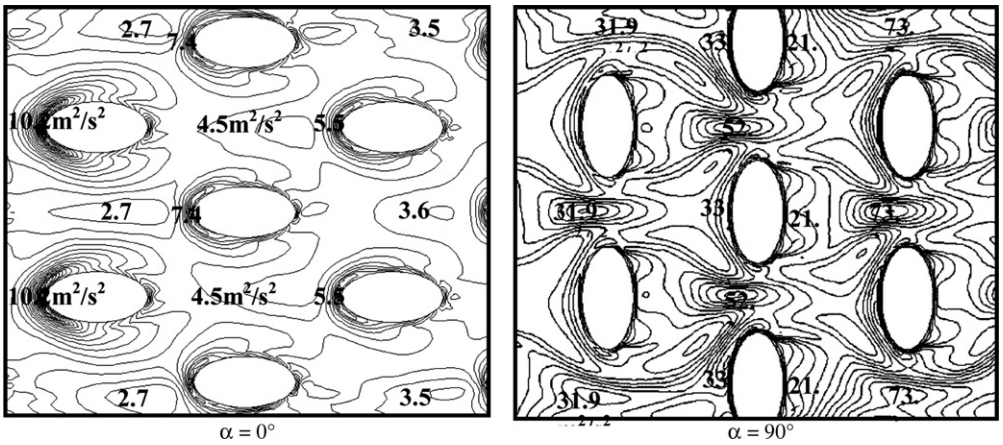

Fig. 5. Turbulent kinetic energy at different angles of attack and $Re = 17{,}000$.

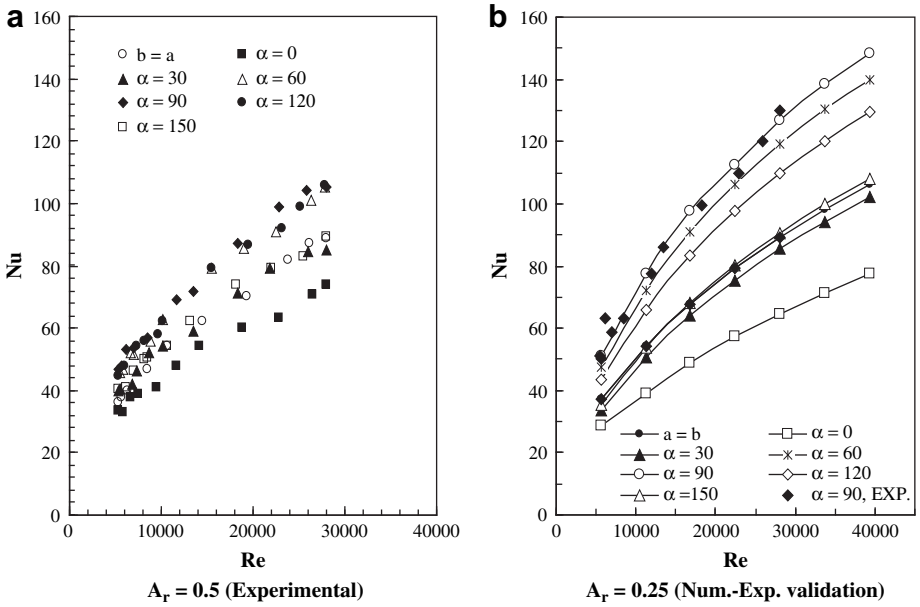

Fig. 6. Nusselt number versus Reynolds number at different tube axis ratios (experimental, numerical-validation).

aerodynamic shape of the elliptic tube with $\alpha = 0^\circ$ which, in turn, produces less drag force.

In practice, the elliptic tube bundle arrangement promoted turbulent mixing and lengthened the air flow-path through tube array. The size and the strength of the turbulence level and reversed flow region are characterized by the angle of attack, the axis ratio and Reynolds number. As the oncoming flow perpendicular to the tube-major axis or close to, the flow passage acts as jet impingement to the next row. The flow passes at the early stage of the thermal boundary-layer development, which enhances the heat transfer coefficient. A higher value of Nusselt number is achieved when the angle of attack tends to be right angle with a lower value of the axis ratio and a higher value of Reynolds number. At these conditions, an increase in the friction factor is a penalty. It is suggested that an appropriate arrangement of the elliptic tubes is required to obtain better global performance, which can be achieved when the flow and the heat transfer resistances are minimized together. An evaluation criterion is required to resort a metric that expresses the heat transfer performance against friction loss performance.

Correlations for both Nusselt number (Eq. (11)) and friction factor (Eq. (12)) were predicted based on experimental results at wide range of validity of different angles of attack, axis ratios and Reynolds numbers with a maximum deviation of ±10% and ±12%, respectively.

$$Nu = 0.452 Re^{0.537} Pr^{0.33} \left(\frac{a}{b}\right)^{-0.079} (\sin(10+\alpha))^{0.2} \tag{11}$$

$$f = 0.195 Re^{-0.0466} Pr^{0.33} \left(\frac{a}{b}\right)^{-2.29} (\sin(10+\alpha))^{0.052} \tag{12}$$

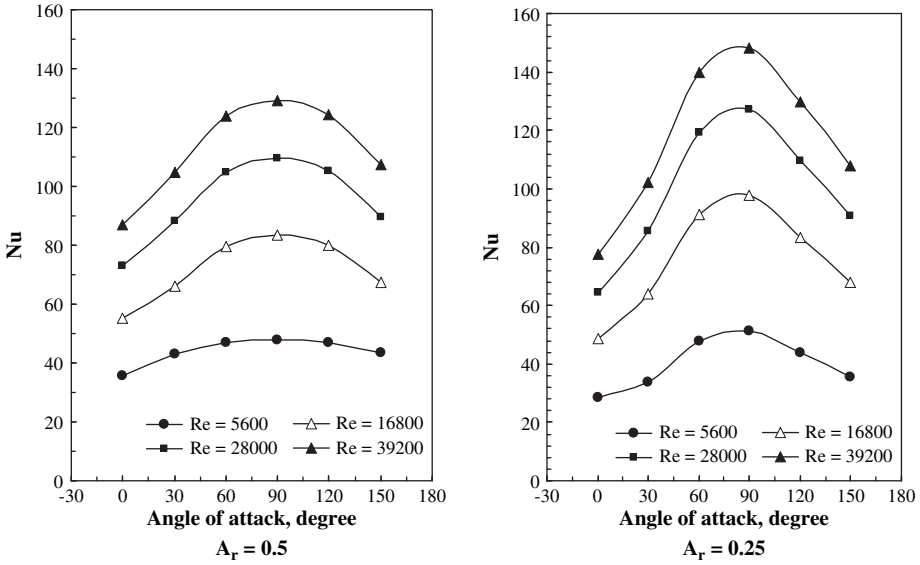

Fig. 7. Nusselt number versus angle of attack at different tube axis ratios (numerical results).

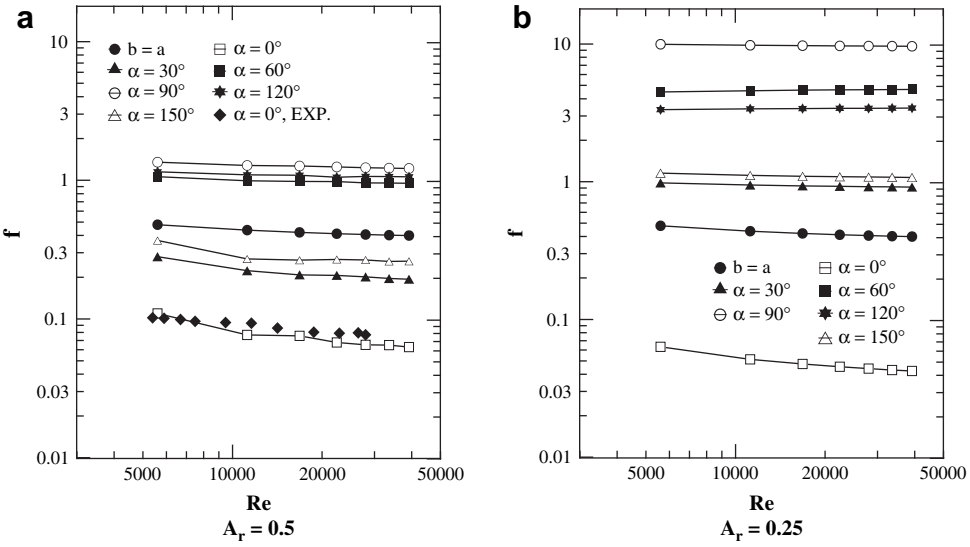

Fig. 8. Friction factor versus Reynolds number at different tube axis ratios (experimental–numerical results validation).

$$5300 \le Re \le 28,000, \quad 0.25 \le \frac{a}{b} \le 1, \quad 0^\circ \le \alpha \le 150^\circ$$

4.2. Thermal performance criteria

Thermal evaluation criteria is very important aspect in the heat exchanger design, since the competing effects of escalating heat transfer as well as increasing pressure drop, make it difficult to determine the relative good of such design. The appropriate selection of the evaluation factor is a point of interest. There are different factors, which enter the decision, making process to use an augmentative technique including heat duty increase, area and pumping power reduction. The thermal evaluation criteria depend on what is held fixed (heat duty, mass flow rate and pressure drop) and what is the desired objective (heat transfer enhancement, frontal area and pumping power reduction). Four methods are presented to resort a metric that expresses the global performance of the elliptic tube bundle heat exchanger with the particular reference of the traditional circular tube bundle. These methods play as key design factors of the heat exchanger whilst incorporating an economic indicator, which are:

1. Direct comparison between the heat transfer coefficient and the pressure drop at a fixed mass flow rate is conducted. This criterion allows quantifying the heat transfer enhancement for different tube bundle configurations with equivalent total pressure drops independently on the tube cross-sectional shape [18].
2. Scope of possible enhancement of the heat transfer per unit pumping power at a fixed mass flow rate, which is expressed by Eq. (13) [19].

$$\varepsilon = \frac{\rho C_p (T_{ao} - T_{ai})}{\Delta P} \tag{13}$$

This criterion is more significant when the overall performance of the heat exchange surfaces is needed, while the cost of the heat transfer enhancement is in the same order of magnitude as the pumping power reduced.

3. The area goodness factor (A_{GF}), which is expressed as the scope of possible reduction of the frontal area of the heat exchanger at a given duty. The tube bundle having a higher "A_{GF}" as the ratio of the Colburn factor to the friction factor is "good" because it requires a lower frontal area of the heat exchanger, Eq. (14) [20].

$$A_{GF} = \left(\sigma^2 j/f\right) = \left(\frac{A_{ff}}{A_{fr}}\right)^2 \left(\frac{Nu}{Re\, Pr^{1/3}}\right)\left(\frac{\rho u_{max}^2 N_R}{2\Delta P}\right) \tag{14}$$

This criterion is more significant when the availability of the space is critical and the heat exchanger size should be minimized for a given heat duty.

4. The efficiency index (η) expresses the heat transfer performance against the friction loss performance of the elliptic tube bundle based on the circular tube bundle performance [21]. The efficiency index (η) is defined as the ratio between the Stanton number enhancement ratio (St/St_o) to the friction factor ratio (f/f_o) at a fixed mass flow rate, Eq. (15).

$$\eta = \frac{(St/St_o)}{(f/f_o)} \tag{15}$$

Fig. 9 shows the heat transfer coefficient versus the pressure drop at different angles of attack with $A_r = 0.5$ and 0.25, respectively under a constant mass flow rate. The maximum heat transfer coefficient (under the constraint of mass flow rate and a fixed pressure drop) is achieved when the oncoming flow is parallel to the tube-major axis ($\alpha = 0^\circ$). While, the worst performance is obtained when the approaching flow is parallel to the tube minor axis ($\alpha = 90^\circ$). Comparing with the circular tube bundle, a better thermal performance of the elliptic tube bundle is achieved when $\alpha = 30^\circ$ or 150° and $0.5 \le A_r \le 0.66$. Conversely, the circular tube bundle has a higher heat transfer coefficient than that of the elliptic tube bundle in the range of $0.25 \le A_r < 0.5$ and $30^\circ < \alpha < 150^\circ$.

The heat transfer enhancement per unit pumping power of the axis ratio = 0.5 is illustrated in Fig. 10. Although the heat exchanger with the angle of attack = 90° having the highest values of Nusselt number, it has the lowest values of the heat transfer per unit pumping power. While the elliptic tube array with the angle of attack = 0° has the highest values of the heat transfer per unit pumping power. The effect of the ellipticity (tube axis ratio) at the optimum angle of attack ($\alpha = 0^\circ$) is presented in Fig. 11. The results

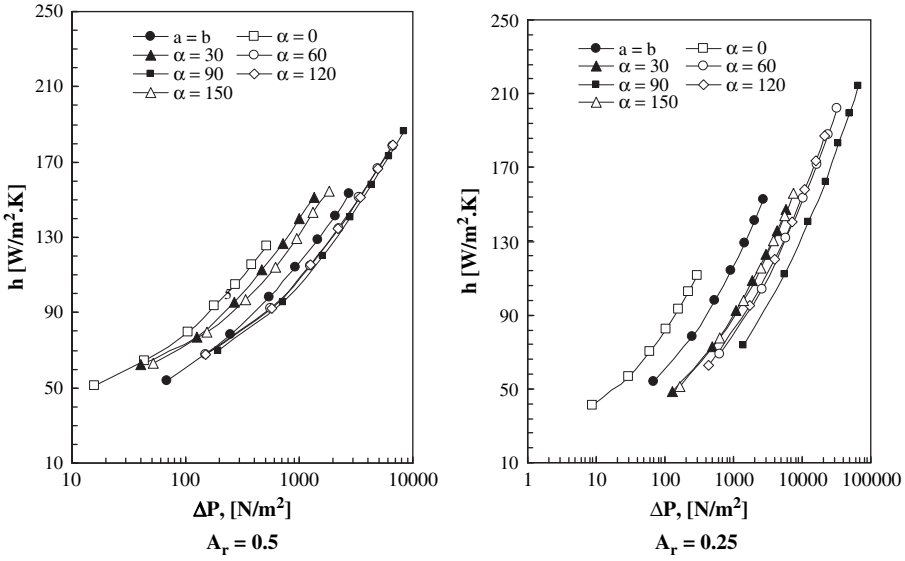

Fig. 9. Heat transfer coefficient versus pressure drop at different tube axis ratios (numerical results).

indicated that, a better thermal performance per unit pumping power of the elliptic tube involving considerable order of magnitude is achieved when compared with the circular tube for all cases of axis ratios. The maximum thermal performance is achieved when the elliptic tube tends to be more flat.

The heat transfer per unit pumping power versus the angle of attack for tube axis ratios = 0.5 and 0.25 is represented in Fig. 12. It is clear that the maximum thermal performance (under constraint of a fixed pumping power) occurred at $\alpha = 0^\circ$ and the minimum thermal performance occurred at $\alpha = 90^\circ$. The best thermal performance of the elliptic tube heat exchanger is qualified at the lower range of Reynolds number, axis ratio and $\alpha = 0^\circ$. To optimize the thermofluid characteristics of heat exchangers, it is important to recognize not only the enhancement of the heat transfer (passive or active techniques) but also the minimization of the pumping power usage. The heat transfer per unit pumping power can be correlated in terms of Reynolds number, Prandtl number, tube axis ratio and the angle of attack with a maximum deviation of ±14% for a wide range of validity as presented in Eq. (16).

$$\varepsilon = 1.41 Re^{-2.65} Pr^{0.33} \left(\frac{a}{b}\right)^{-1.11} (\sin(\alpha + 10))^{-15.33} \tag{16}$$

$$5600 \le Re \le 40,000, \quad 0.25 \le \frac{a}{b} \le 1, \quad 0^\circ \le \alpha \le 150^\circ$$

The scope of possible reduction of the frontal area of the heat exchanger for a given duty, which is expressed as the area goodness factor is introduced. Fig. 13 shows the area goodness factor versus Reynolds number for axis ratios = 0.5 and 0.25, respectively. Based on the circular tube, the elliptic tube with

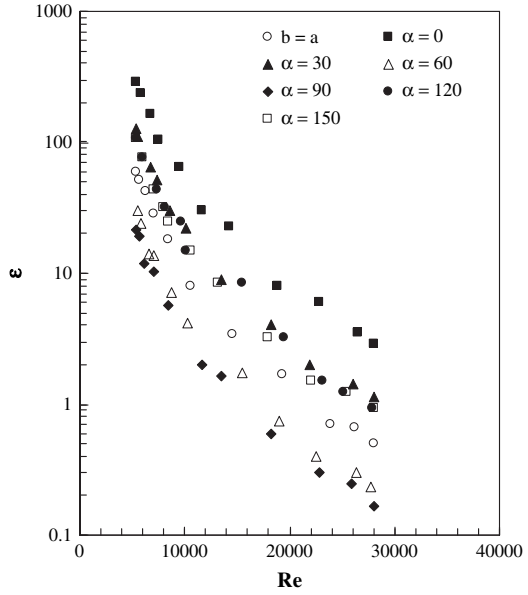

Fig. 10. Heat transfer per unit pumping power for tube axis ratio = 0.5 (experimental results).

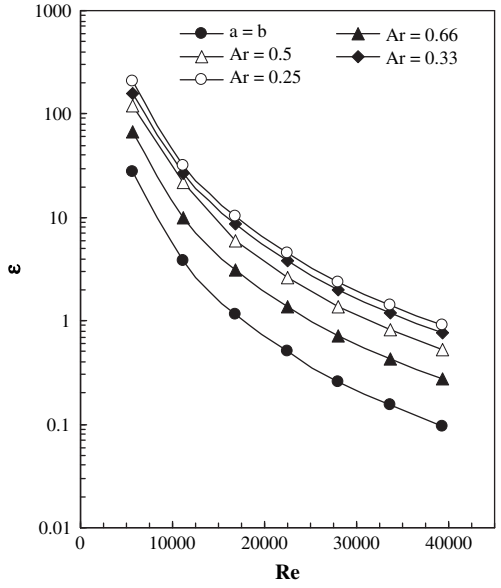

Fig. 11. Heat transfer per unit pumping power for angle of attack = 0° (numerical results).

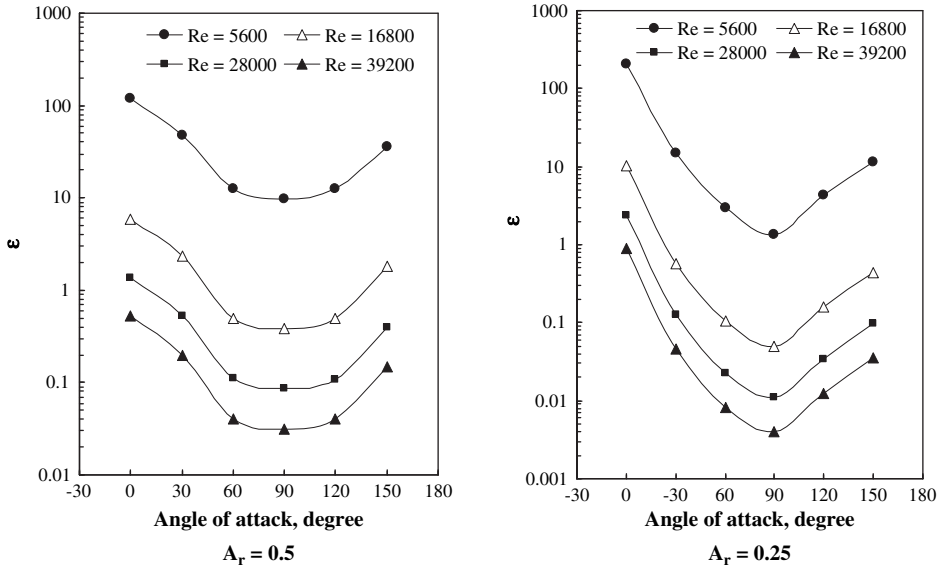

Fig. 12. Heat transfer per unit pumping power versus angle of attack at different axis ratios (numerical results).

zero angle of attack has a maximum area goodness factor for all values of axis ratio. A better area goodness factor can be obtained also with the elliptic tube having $\alpha = 30^\circ$ and 150° when the axis ratio ranges from 0.5 to 0.66. The elliptic tube bundle produced a considerable frontal area reduction of heat exchanger at $\alpha = 0^\circ$ with $0.25 \le A_r < 1$, as well as at $\alpha = 30^\circ$ with $0.5 \le A_r \le 0.66$. These results permitted also a possible reduction to the transfer surface area when fins attached to the tube and hence saving materials, which is pronounced to a manufacturing cost of the heat exchanger.

The heat transfer performance against the friction loss performance of the elliptic tube bundle based on the circular tube bundle performance which is expressed as the efficiency index (η) is presented. The ratios between the Stanton number enhancement ratio (elliptic/circular) and the friction factor ratio (elliptic/circular) at the same mass flow rate versus Reynolds number are illustrated in Fig. 14. It is evident that the elliptic tube with zero angle of attack has the highest value of efficiency index for the axis ratio range of $0.25 \le A_r < 1$ followed by the angle of attack $= 30^\circ$ for the axis ratio range of $0.5 \le A_r \le 0.66$. The heat exchangers employing elliptic tube arrangement contribute significantly to the energy conservation. In most applications, the heat exchanger is a part of the whole thermal system and hence the qualitative and quantitative assessments of this energy conservation come together with the overall evaluation of the energy consumption by the system.

5. Conclusions

The thermal performance criterion of the elliptic tube bundle heat exchanger in crossflow has been quantitatively addressed. Experimental and numerical investigations of the turbulent flow through bundle of elliptic tubes heat exchangers were carried out. The investigation covers the effects of key design parameters of Reynolds number, minor-to-major axis ratio, and flow angle of

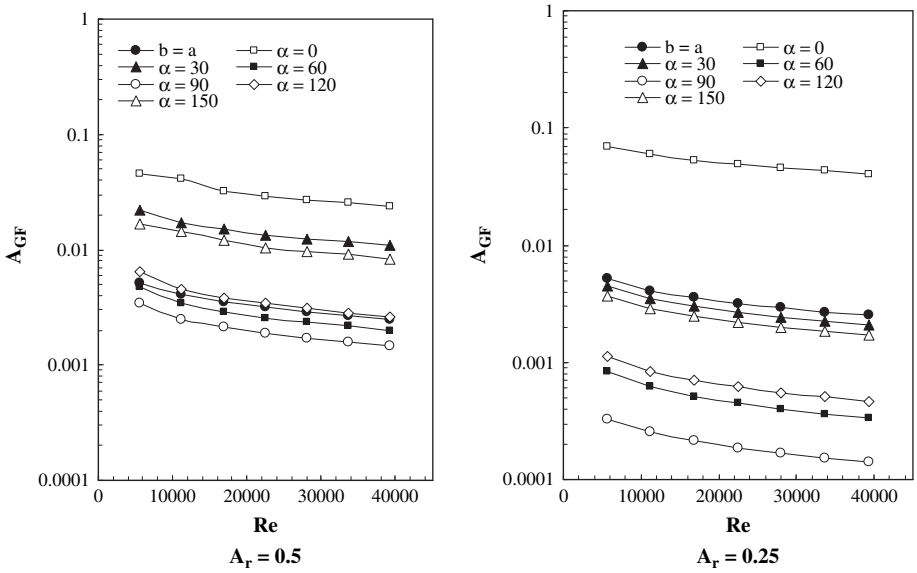

Fig. 13. Area goodness factor versus Reynolds number at different tube axis ratios (numerical results).

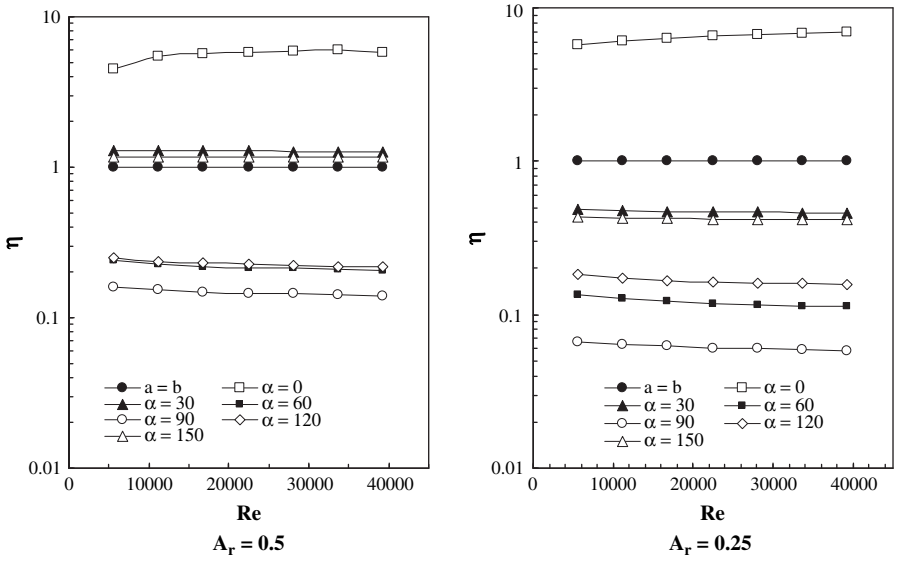

Fig. 14. Efficiency index versus Reynolds number at different tube axis ratios (numerical results).

attack. Four methods are presented to resort a metric that expresses the thermal performance criteria of the elliptic tube bundle with the particular reference of the traditional circular tube bundle. These methods are depending on what is held fixed (heat duty, mass flow rate and pressure drop) and what is the desired objective (heat transfer enhancement, frontal area and pumping power reduction). Correlations of Nusselt number, friction factor as well as the heat transfer per unit pumping power against design parameters are presented.

The main conclusions are:

1. The increase of angle of attack clockwise until 90° enhances the convective heat transfer coefficient considerably. The maximum heat transfer coefficient at a certain mass flow rate is achieved when the oncoming flow is parallel to the major axis of the tube ($\alpha = 0^\circ$) while, the worst performance is obtained when the oncoming flow is parallel to tube minor axis ($\alpha = 90^\circ$).
2. The elliptic tube bundle with zero angle of attack has the maximum area goodness factor for all values of axis ratios followed by the angle of attack = 30° for a given duty. This produced a considerable frontal area reduction of the heat exchanger, which is also permitted to a possible reduction of the transfer surface area when fins are attached to the tube.
3. The maximum thermal performance under a fixed pumping power is obtained at $\alpha = 0^\circ$ and the minimum thermal performance occurred at $\alpha = 90^\circ$. The best thermal performance of the elliptic tube heat exchanger is qualified with the lower values of Reynolds number, axis ratio and zero angle of attack.
4. The elliptic tube heat exchanger with zero angle of attack has the highest value of the efficiency index for the axis ratio ranges $0.25 \le A_r < 1$ followed by the angle of attack = 30° for the axis ratio ranges $0.5 \le A_r \le 0.66$.
5. The heat exchanger employing elliptic tube arrangement contributes significantly to the energy conservation.

References

[1] O. Terukazu, N. Hideya, T. Yukiyasu, Heat transfer and flow around an elliptic cylinder, Int. J. Heat Mass Transfer 27 (10) (1984) 1771–1779.
[2] J. Jang, B. Li, A numerical analysis of two-dimensional laminar flow over an elliptic tube bank, in: 4th Int. Symp. on Heat Transfer, Beijing, China, 1996, pp. 547–552.
[3] L.A.O. Rocha, F.E.M. Saboya, J.V.C. Vargas, A comparative study of elliptical and circular sections in one- and two-row tubes and plate fin heat exchangers, Int. J. Heat Fluid Flow 18 (2) (1997) 247–252.
[4] H.M. Badr, Forced convection from a straight elliptical tube, J. Heat Mass Transfer 34 (2–3) (1998) 229–236.
[5] R.S. Matos, J.V.C. Vargas, T.A. Laursen, F.E.M. Saboya, Optimization study and heat transfer comparison of staggered circular and elliptic tubes in forced convection, Int. J. Heat Mass Transfer 44 (2001) 3953–3961.
[6] D. Bouris, G. Papadakis, G. Bergeles, Numerical evaluation of alternate tube configurations for particle deposition rate reduction in heat exchanger tube bundles, Int. J. Heat Fluid flow 22 (5) (2001) 525–536.
[7] D.K. Harris, V.W. Goldschmidt, Measurements of the overall heat transfer from combustion gases confined within elliptical tube heat exchangers, Exp. Therm. Fluid Sci. 26 (1) (2002) 33–37.
[8] M.G. Khan, A. Fartaj, D.S.K. Ting, An experimental characterization of cross-flow cooling of air via an in-line elliptical tube array, Int. J. Heat Fluid Flow 25 (4) (2004) 636–648.
[9] R.S. Matos, T.A. Laursen, J.V.C. Vargas, A. Bejan, Three-dimensional optimization of staggered finned circular and elliptic tubes in forced convection, Int. J. Therm. Sci. 43 (2004) 477–487.
[10] R.S. Matos, J.V.C. Vargas, T.A. Laursen, A. Bejan, Optimally staggered finned circular and elliptic tubes in forced convection, Int. J. Heat Mass Transfer 47 (2004) 1347–1359.
[11] Z. Li, J.H. Davidson, S.C. Mantell, Numerical simulation of flow field and heat transfer of streamlined cylinders in crossflow, J. Heat Transfer 128 (6) (2006) 564–570.
[12] B. Li, B. Feng, Y.L. He, W.Q. Tao, Experimental study on friction factor and numerical simulation on flow and heat transfer in an alternating elliptical axis tube, Appl. Therm. Eng. 26 (17–18) (2006) 2336–2344.
[13] Y.B. Tao, Y.L. He, Z.G. Wu, W.Q. Tao, Three-dimensional numerical study and field synergy principle analysis of wavy fin heat exchangers with elliptic tubes, Int. J. Heat Fluid Flow 28 (6) (2007) 1531–1544.
[14] J.P. Holman, Experimental Methods for Engineers, seventh ed. McGraw-Hill Int., New York, USA, 2001.
[15] FLUENT, User's Manual, Fluent Inc., USA, 2005.
[16] V. Gnielinski, New equations for heat and mass transfer in turbulent pipe and channel flow, Int. Chem. Eng. 16 (1976) 359–367.
[17] B.E. Launder, T.H. Massey, The numerical prediction of viscous flow and heat transfer in tube banks, J. Heat Transfer ASME Trans. 100 (1978) 565–571.
[18] A. Bergles, A. Blumenkra, J. Taborek, Performance evaluation criteria for enhanced heat transfer surfaces, in: 4th Int. Heat Transfer Conference, vol. 2, 1974, pp. 239–243.
[19] A. Gomaa, R. LeFeuvre, C. Underwood, T. Bond, Numerical analysis of developing laminar flow and heat transfer characteristics through corrugated wall channels, in: IMechE 6th UK National Conference on Heat Transfer, UK, 1999, pp. 205–214.
[20] W.M. Yan, P.J. Sheen, Heat transfer and friction characteristics of fin-and-tube heat exchangers, Int. J. Heat Mass Transfer 43 (9) (2000) 1651–1659.
[21] R. Afify, N. Berbish, A. Gomaa, A. Eid, Numerical and experimental study of turbulent flow and convective heat transfer in a circular tube with disc-baffles, Engineering Research Journal 96 (2004) M37–M61 Faculty of Eng. at Mattaria, Egypt.